International Journal of Nanomedicine

Dovepress
open access to scientific and medical research

Open Access Full Text Article

ORIGINAL RESEARCH

A ^{89}Zr-labeled lipoplex nanosystem for image-guided gene delivery: design, evaluation of stability and in vivo behavior

This article was published in the following Dove Press journal:
International Journal of Nanomedicine

Istvan Hajdu[1]
Amal Makhlouf[1,2]
Viswas Raja Solomon[3]
Deborah Michel[1]
Mays Al-Dulaymi[1]
Kishor M Wasan[1]
Humphrey Fonge[3,4]
Ildiko Badea[1]

[1]Drug Discovery and Development Research Group, College of Pharmacy and Nutrition, University of Saskatchewan, Saskatoon, SK S7N 5E5, Canada; [2]Department of Pharmaceutics and Industrial Pharmacy, Faculty of Pharmacy, Cairo University, 12411 Cairo, Egypt; [3]Department of Medical Imaging, College of Medicine, University of Saskatchewan, Saskatoon, SK S7N 0W8, Canada; [4]Department of Medical Imaging, Royal University Hospital Saskatoon, SK S7N 0W8, Canada

Correspondence: Humphrey Fonge
Department of Medical Imaging, College of Medicine, University of Saskatchewan, 103 University Drive, Saskatoon, SK S7N 0W8, Canada
Tel +1 306 655 3353
Email humphrey.fonge@usask.ca

Ildiko Badea
Drug Discovery and Development Research Group, College of Pharmacy and Nutrition, University of Saskatchewan, 107 Wiggins Road, Saskatoon, SK S7N 5E5, Canada
Tel +1 306 966 6349
Fax +1 306 966 6377
Email ildiko.badea@usask.ca

Background: With the advances in radiopharmaceutical research, the development of image-guided therapy has become a major interest. While the development of theranostic nanotherapeutics is frequently associated with cancer chemotherapy, phototherapy and radiotherapy, there is little information available on the in vivo monitoring of gene delivery systems and the application of image-guided approach in gene therapy. The goal of this work was to determine the in vivo behavior of DNA delivery nanosystems - based on cationic gemini surfactants – designed for image-guided gene therapy. We tested the feasibility of monitoring tumor accumulation of gene delivery nanoparticles by positron emission tomography.

Methods: To be able to conjugate radiotracers to the nanoparticles, a deferoxamine-modified gemini surfactant was synthesized, DNA-containing lipoplex nanoparticles were formulated, and radiolabeled with Zirconium-89 (^{89}Zr). The pharmacokinetics and biodistribution of ^{89}Zr labeled surfactant and ^{89}Zr labeled nanoparticles were monitored in mice by microPET/CT imaging and ex vivo gamma counting.

Results: Modification of the nanoparticles with deferoxamine did not alter their physicochemical properties. The radiolabeled nanoparticles (labeling efficiency of 95±3%) were stable in PBS and serum. The biological half-life of the ^{89}Zr labeled nanoparticles was significantly higher compared to ^{89}Zr labeled surfactant. As expected, the nanoparticles had significantly higher liver accumulation than the radiolabeled surfactant alone and lower kidney accumulation. Tumor uptake was detected at 2 hours post injection and decreased throughout the 3-day monitoring.

Conclusion: We propose that radiolabeling DNA delivery lipoplex nanosystems is a promising approach for the design and optimization of image-guided nanomedicines, especially in the context of cancer gene therapy.

Keywords: gemini surfactant, pharmacokinetic, biodistribution, melanoma, microPET imaging

Introduction

The development of nanotechnology has a major contribution in the progress of molecular imaging and targeted therapy of cancers.[1,2] As imaging and therapeutic agents, nanoparticles offer numerous advantages such as increased tissue permeability, controlled release, improved biodistribution, modified pharmacokinetics and ability to target specific tissues.[3] The number of nanoparticle-based medicaments is increasing in clinical trials and on the market, because the efficacy of these nanomedicines can considerably exceed the efficacy of the conventional medicines.[4,5] The overall approach is to use targeted nanoparticles as carriers, for both therapeutic and contrast agents, delivering their cargo in higher concentration to the desired location resulting

submit your manuscript | www.dovepress.com
Dovepress
http://dx.doi.org/10.2147/IJN.S179806

in higher tumor-to-background ratio, better contrast and more selective tumor identification.[6,7] The importance of nanoparticles has increased remarkably in the past decades[8] due to their outstanding biological compatibility and in vivo stability.[9] Among the nanosized systems, liposomes and other lipid-based systems have been used more than four decades as vehicles for drug delivery and, more recently, as molecular imaging agents in the field of oncology.[10–12]

To capitalize on the advantages of the lipid-based nanoparticles, recent advances in nanoparticle technology explore the combination of therapeutic and diagnostic agents in a single particle,[13] ideal for personalized medicine.[14] The benefit of creating multifunctional nanoparticles – by incorporating both drugs and imaging agent into a single nanomedicine – is that drug localization and therapeutic efficacy can be monitored simultaneously in a noninvasive manner,[15] developing the field of image-guided therapy.[16]

Radiolabeled nanoparticles represent a new type of agent with great potential for clinical applications. The surface of these nanoparticles can be functionalized with imaging and targeting agents and, by virtue of their improved in vivo stability and enhanced permeation and retention effects, they can be used to improve the specificity and sensitivity of imaging technologies.[17] Liposomes have been frequently employed to deliver imaging radionuclides for positron emission tomography (PET)[18] or single-photon emission computed tomography.[19,20] Multifunctional liposomes labeled with radiometals, such as ^{64}Cu ($t_{1/2}$=12.7 hours)[21,22] and ^{89}Zr ($t_{1/2}$=78.41 hours),[23,24] for PET imaging showed high tumor accumulation due to the unique properties and high specificity.

Development of biotechnology products, such as genetic material-based drugs, could greatly benefit from radiolabeling nanoparticulate delivery systems. While the benefits of gene therapy in numerous inherited and acquired diseases and in development of novel vaccines are evident, there are two major hurdles this area of research needs to overcome.

The first barrier in gene therapy aiming to restoration or blocking of a specific gene function is the development of safe and efficient gene delivery systems. Cationic liposomes are the most researched nonviral polycationic systems, which compact negatively charged nucleic acids leading to the formation of lipoplexes. They have unique characteristics, such as capability to incorporate DNA/RNA, low toxicity, no activation of immune system and the amenability for targeted delivery of bioactive compounds to the site of action.[25] Lipoplexes are considered as alternative gene therapy for cancer.[26–28] Numerous reports have highlighted the antitumor effect of these gene therapy systems.[29–31] Gemini cationic surfactants are one of the cationic lipid families that assemble into nanosized lipoplexes of various morphologies. They have multipurpose chemical structure with two alkyl tails attached to quaternary ammonium groups and connected with a functionalizable spacer. They are able to compact the genetic material into 100–150 nm size lipoplex particles with positive surface charge,[32] which enables interaction with the cell surface and endocytosis. In addition, the gemini surfactants protect DNA/RNA from premature degradation by endonucleases. In our previous work, physicochemical and interfacial properties,[33,34] efficiency and safety of gene delivery,[35] stability of the DNA delivery system[36] was demonstrated.

The second barrier to the clinical translation of gene therapy is the lack of appropriate monitoring of the biological fate of the lipoplex nanoparticles and therapeutic outcome. Thus, combination of lipoplexes and radiolabeling opens new opportunities in the field of image-guided therapy and theranostics. Lipoplexes can be effectively labeled with radionuclides, which facilitate evaluation of the fate of these gene delivery nanosystems in real-time noninvasively using nuclear imaging techniques. To monitor the biological fate of these nanoparticles, ^{89}Zr was selected as an appropriate radionuclide, because the decay half-life of ^{89}Zr ($t_{1/2}$=78.41 hours) is appropriate for monitoring the biological fate of nanoparticles[37] rendering PET imaging with ^{89}Zr-labeled agents a highly dynamic research area.[38,39]

In the present study, nanoparticle labeling, gene expression properties, in vitro stability and in vivo biodistribution and tumor uptake of these novel ^{89}Zr-radiolabeled lipoplex nanoparticles were performed and described. The gene expression and cell viability of A375 cells were investigated in vitro after treated with lipoplex nanoparticles. Pharmacokinetic profile and the biodistribution of the radiolabeled lipoplex nanosystem compared with the radiolabeled gemini surfactants were specified in vivo using healthy athymic CD-1 nude mice. This system was used for the assessment of the kinetics, distribution in the living body and tumor deposition of lipoplex nanoparticles. To our knowledge, this is the first report on the use of ^{89}Zr-labeled gene delivery nanoparticles and the first evidence that this gene delivery system could be monitored by radiolabeling, therefore, show a potential for the development of image-guided gene therapy.

Materials and methods

Materials

3,3′-Iminobis(*N*,*N*-dimethylpropylamine), Boc-Gly-OH, Fmoc-Lys(Boc)-OH, and 1-Iodododecane were purchased from Sigma-Aldrich Co. (St Louis, MO, USA); *N*,*N*′-

Diisopropylethylamine (DIPEA) and O-(7-Azabenzotriazol-1-yl)-*N*,*N*,*N*′,*N*′-tetramethyluronium hexafluorophosphate (HATU) were purchased from Chem-Impex International, Inc (Wood Dale, IL, USA); 1,2-dioleoyl-sn-glycero-3-phosphoethanolamine (DOPE) was purchased from Avanti Polar Lipids, Inc (Alabaster, AL, USA) and p-SCN-Bn-Deferoxamine (deferoxamine) was purchased from Macrocyclics, Inc (Cat. No: B-705) (Dallas, TX, USA). All other chemicals, unless otherwise noted, were used of the highest grade and purchased from Sigma-Aldrich. These chemicals were used without further purification. The water used in the process was ultrapure obtained in a MilliQ system (resistance of >18.18 MΩ cm at 25°C) and the dimethyl sulfoxide (DMSO) was of molecular biology grade (>99.9%). The construction of the plasmid pGTh-CMV. IFN-GFP (pDNA), encoding for murine interferon gamma (IFN-γ) and green fluorescent protein (GFP) was described previously.[32] The p-DNA for this study was selected as a robust model used in previous work and will be replaced with specific tumor suppressor genes for functional studies.

^{89}Zr was purchased from Washington University (St Louis, MO, USA). Activity measurements were made using a Biodex Atomlab 500 Dose Calibrator (Shirley, NY, USA). For accurate quantification of activities, samples were counted for 1 minute on a calibrated Perkin-Elmer Automatic Wizard^2 Gamma Counter (Waltham, MA, USA). Labeling of gemini surfactants and liposomes with ^{89}Zr was monitored using silica-gel impregnated glass-fiber instant thin layer chromatography (ITLC-SG) (Agilent Technologies, Santa Clara, CA, USA).

Mass spectra were obtained using a QSTAR XL MS/MS system. ^{1}H NMR spectra, in D_2O, $CDCl_3$ or DMSO-d_6, were recorded using a Bruker 500 MHz Avance spectrometer. Chemical shifts, δ, are reported in parts per million, referenced to the residual ^{1}H and ^{13}C (D_2O at 4.80, $CDCl_3$ at 7.26, 77.23 and DMSO-d_6 at 2.50, 39.58), respectively. Purity of the compounds was further verified by reversed-phase (RP) HPLC (RP-HPLC) using an Agilent 1200 Series HPLC coupled to a UV detector and Waters 2796 HPLC System coupled to an UV and radiometric detector.

Synthesis

All reactions (Figure 1) were carried out under a nitrogen atmosphere using standard Schlenk techniques.

Step a: In a dry Schlenk flask, Boc-Gly-OH (8.65 mmol) was dissolved in dry *N*,*N*-Dimethylformamide (DMF) (10 mL), followed by the addition of HATU (10.4 mmol) and DIPEA (17.3 mmol). The reaction mixture was then cooled and stirred for 15 minutes before the addition of

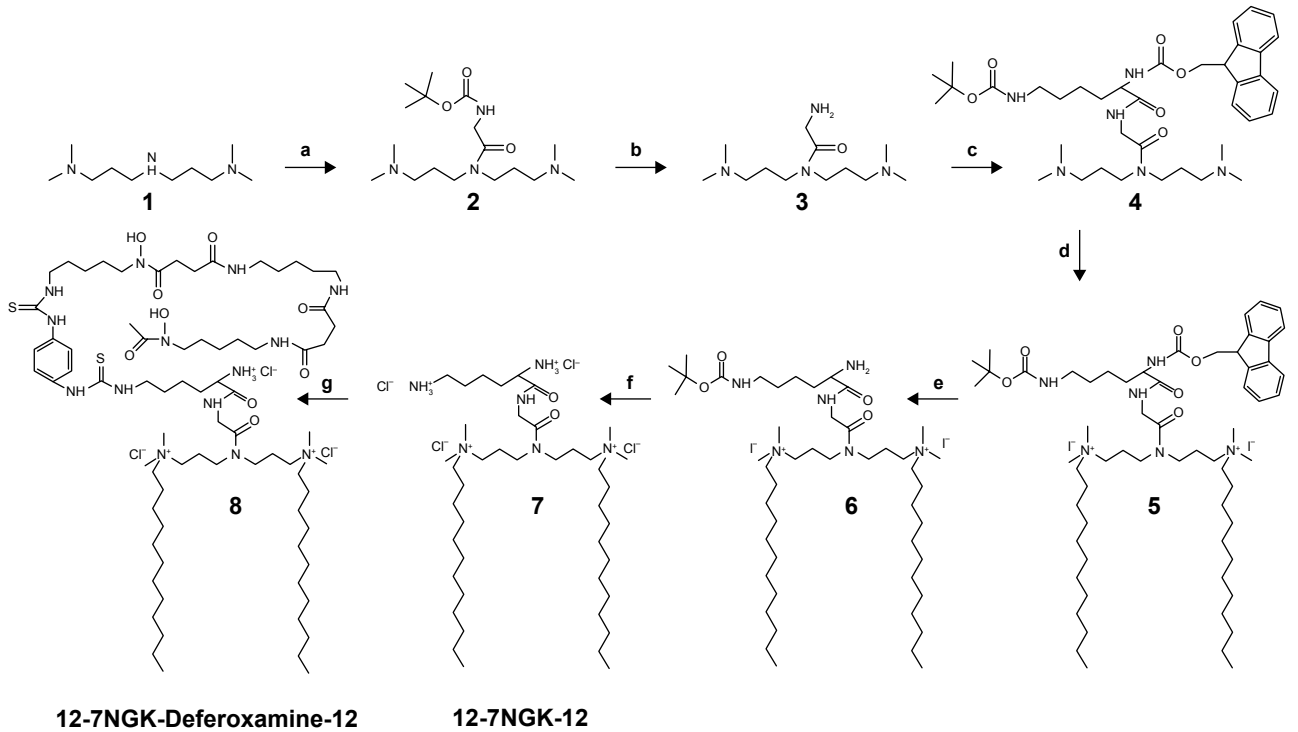

Figure 1 Structure and synthetic scheme of glycine-lysine substituted gemini surfactant (12-7NGK-12) and deferoxamine-modified gemini surfactant (12-7NGK-Deferoxamine-12).

Notes: a: conjugation of the 3-carbon linker group on the spacer of the gemini surfactant; b: removal of protection; c: conjugation of protected lysine on the spacer; d: addition of the tail of the gemini surfactant; e: deprotection; f: deprotection and ion exchange; and g: conjugation of deferoxamine.

3,3′-Iminobis(*N*,*N*-dimethylpropylamine) (8.3 mmol). After 24 hours, DMF was removed from the reaction mixture under high vacuum, and the sample was dissolved in dichloromethane (DCM) (100 mL) and extracted with a saturated aqueous solution of sodium bicarbonate (5×100 mL). Then, the aqueous layer was washed with DCM (5×75 mL). The collected organic phase was dried with sodium sulfate before removing the DCM under vacuum. A yellow oily compound, *N*-2-(tert-butyloxycarbonyl) amino-*N*,Nbis[3-(dimethylamino)propyl]-acetamide (**2**), was obtained. ^{1}H NMR ($CDCl_3$) δ/ppm: 5.55 (brs, 1H), 3.99–3.96 (m, 2H), 3.40–3.22 (m, 4H), 2.35–2.16 (m, 16H), 1.76–1.67 (m, 4H), 1.43 (s, 9H). Yield was 76%.

Step b: 8.7 mmol of (**2**) was dissolved in 10 mL of DCM, followed by the addition of 10 equivalents of HCl (4 M in dioxane) for 90 minutes. After that, the solvent was removed from the reaction mixture under vacuum. The solid residue was dissolved in 30 mL DCM and 3.5 equivalents of DIPEA, added dropwise. After 90 minutes stirring, the solvent was removed under vacuum. A yellow solid compound, *N*-2-amino-*N*,*N*-bis[3-(dimethylamino)-propyl]-acetamide (**3**), was obtained. ^{1}H NMR ($CDCl_3$) δ/ppm: 5.70 (m, 2H), 3.96 (m, 2H), 3.36 (m, 2H), 3.24 (m, 2H), 2.32 (m, 4H), 2.26–2.16 (m, 12H), 1.74–1.64 (m, 4H). Yield was 92%.

Step c: Fmoc-Lys(Boc)-OH (11.75 mmol) was dissolved in 20 mL dry DMF, followed by the addition of HATU (14.1 mmol) and DIPEA (23.45 mmol). The reaction mixture was then cooled and stirred for 15 minutes before the addition of *N*-2-amino-*N*,*N*-bis[3-(dimethylamino)-propyl]-acetamide (**3**) (11.25 mmol). After 24 hours, the DMF was removed from the reaction mixture under high vacuum, and the residue was dissolved in DCM (100 mL) and extracted with a saturated aqueous solution of sodium bicarbonate (5×100 mL). Then the aqueous layers were washed with DCM (5×100 mL). The collected organic phase was dried with sodium sulfate before removing the DCM under vacuum. A yellow oily compound, (9H-fluoren-9-yl)methyl tert-butyl (6-((2-(bis(3-(dimethylamino)propyl)amino)-2-oxoethyl)amino)-6-oxohexane-1,5-diyl)dicarbamate (4), was obtained. ^{1}H NMR ($CDCl_3$) δ/ppm: 7.76–7.66 (m, 4H), 7.36 (m, 2H), 7.30 (m, 2H), 4.4–4.1 (m, 4H), 3.45 (m, 4H), 3.28 (m, 2H), 3.08 (m, 4H), 2.76 (m, 12H), 2.33–2.23 (m, 4H), 1.42 (m, 9H), 1.24 (m, 10H). Yield was 77%.

Step d: 1.43 mmol of (**4**) was dissolved in 15 mL dry DMF and 1-Iodododecane (3.57 mmol) was added dropwise. The reaction mixture was stirred for 18 hours at room temperature. After 18 hours, DMF was removed from the reaction mixture under high vacuum. The residue was washed five times with 25 mL diethyl-ether and the diethyl-ether was removed with vacuum. 10-((((9H-fluoren-9-yl)methoxy)carbonyl)amino)-*N*-dodecyl-15-(3-(dodecyldimethylammonio) propyl)-*N*,*N*,2,2-tetramethyl-4,11,14-trioxo-3-oxa-5,12,15-triazaoctadecan-18-aminium iodide (**5**). ^{1}H NMR ($CDCl_3$) δ/ppm: 7.76–7.66 (m, 4H), 7.36 (m, 2H), 7.30 (m, 2H), 4.4–4.1 (m, 4H), 3.45 (m, 4H), 3.28 (m, 2H), 3.08 (m, 4H), 2.76 (m, 12H), 2.33–2.23 (m, 4H), 1.80 (m, 3H), 1.56 (m, 6H), 1.48 (m, 6H) 1.42 (m, 12H), 1.24 (m, 35H), 0.86 (t, 6H). Yield was 72%.

Step e: 0.967 mmol of (**5**) was dissolved in 15 mL dry DMF and 15 mL of piperidine was added dropwise. The reaction mixture was stirred for 18 hours at room temperature. After 18 hours, DMF/piperidine was removed under high vacuum. The residue was washed five times with 25 mL ethyl-acetate and the ethyl-acetate was removed with vacuum. 10-amino-*N*-dodecyl-15-(3-(dodecyldimethylammonio) propyl)-*N*,*N*,2,2-tetramethyl-4,11,14-trioxo-3-oxa-5,12,15-triazaoctadecan-18-aminium (**6**). ^{1}H NMR ($CDCl_3$) δ/ppm: 4.09 (m, 2H), 3.45 (m, 4H), 3.28 (m, 2H), 3.08 (m, 4H), 2.76 (m, 12H), 2.33–2.23 (m, 4H), 1.80 (m, 3H), 1.56 (m, 6H), 1.48 (m 6H) 1.42 (m, 12H), 1.24 (m, 35H), 0.86 (t, 6H). Yield was 83%.

Step f: 0.739 mmol (**6**) was dissolved in 10 mL DCM. 10 equivalents of HCl (4 M in dioxane) was added and stirred for 90 minutes at room temperature. Solvent was removed from the reaction mixture under vacuum. The crude compound was washed ten times with acetone and pure solid 6-((2-(bis(3-(dodecyldimethylammonio)propyl)amino)-2-oxoethyl)amino)-6-oxohexane-1,5-diaminium chloride, 12-7NGK-12 (**7**) gemini surfactant was obtained. ^{1}H NMR (500 MHz, D_2O) δ/ppm, 4.25 (m, 2H), 4.15 (brs, 1H), 3.52 (m, 4H), 3.35 (m, 4H), 3.17–3.00 (m, 12H), 2.96 (s, 2H), 2.93 (s, 2H), 2.26–1.88 (m, 8H), 1.76 (m, 11H), 1.52 (brs, 5H), 1.32 (m, 33H), 0.90 (t, 6H). Yield was 88%.

Step g: 0.070 mmol of (**7**) was dissolved in 2 mL DCM and 25 µL DIPEA was added and stirred for 1 hour. The DCM was removed under vacuum and the residue was dissolved in 2 mL DMSO. Deferoxamine 0.056 mmol was added to the solution and the pH of the solution was adjusted to 8.5 by adding DIPEA. The mixture was stirred for 24 hours. The solvent was removed under vacuum and the product was purified by flash column chromatography (C18-RP silica-gel particle size 15–25 µm) eluting with water/acetonitrile. The appropriate fraction was verified with high-resolution mass spectrometry (MS) and freeze dried to obtain the *N*,*N*′-(((2-(2-amino-6-(3-(4-(3-(3,14,25-trihydroxy-2,10,13,21,24-pentaoxo-3,9,14,20-tetraazatriacontan-30-yl)

thioureido)phenyl)thioureido)hexanamido)acetyl)azanediyl) bis(propane-3,1-diyl))bis(*N*,*N*-dimethyldodecan-1-aminium) chloride, 12-7NGK-Deferoxamine-12, (**8**) deferoxamine-modified gemini surfactant solid product. The purity was further verified on RP-HPLC using Phenomenex Gemini-NX (Phenomenex, Torrance, CA, USA) C18 analytical column (3 µm, 4.6×150 mm). Gradient elution was performed at a flow rate of 1 mL/min using an Agilent 1200 Series HPLC System. Detection was performed using an Agilent absorbance detector at 254 nm. The mobile phase consisted of 0.1% trifluoroacetic acid in H_2O (solution A) and 0.1% trifluoroacetic acid in acetonitrile (solution B). The mobile phase was programmed as follows: gradient from 90% A:10% B to 10% A:90% B in 30 minutes.

12-7NGK-Deferoxamine-12: ^{1}H NMR (500 MHz, DMSO-d_6) δ/ppm, 9.68 (m, 2 hours), 8.2 (m, 1H), 7.8 (m, 4H), 7.44–7.32 (m, 3H), 3.48 (m, 40H), 3 (m, 10H), 2.76 (m, 2H), 2.58 (m, 2H), 2.50 (m, 17H), 2.28 (m, 3H), 1.96 (s, 3H), 1.66 (m, 2H), 1.56–1.48 (m, 8H), 1.38 (m, 4H), 1.24 (m, 36H), 0.86 (t, 6H). Yield was 63%.

Formulation of the lipoplex nanoparticles

The standard nanoparticle formulation was described earlier.[35,36] Briefly, in step 1, plasmid–gemini surfactant complexes were created by mixing an aqueous solution of pDNA with an appropriate amount of 3 mM gemini surfactant solution at 1:5 phosphate to nitrogen ratio and incubated at room temperature for 20 minutes. In step 2, lipoplex nanoparticles were formulated by mixing plasmid–gemini surfactant complexes with the DOPE (1 mM) vesicles at gemini surfactant to DOPE molar ratio of 1:10 and incubated at room temperature for 20 minutes. For the preparation of deferoxamine-modified lipoplex nanoparticles, a predetermined amount (2.5%, 5%, 7.5% and 10%) of gemini surfactant was replaced with the deferoxamine-modified gemini surfactant (which amounts to a 0.25%–1% final concentration of the total lipids, Figure 2).

Radiolabeling and characterization

For radiolabeling, the deferoxamine-modified gemini surfactant was dissolved in HEPES buffer (pH 7.4) in 3 mM concentration. [^{89}Zr] Zr-oxalate 10–15 MBq (300–400 µCi) in oxalic acid was diluted with 20–30 µL HEPES buffer and was adjusted to pH 7.0–7.5 with 2.0 M Na_2CO_3. After the evolution of CO_2 (g), the surfactant solution was added to ^{89}Zr solution, and the labeling solution was incubated at 37°C for 1 hour resulting in the formation of ^{89}Zr-labeled gemini surfactant (^{89}Zr-Surfactant). For nanoparticle labeling, the [^{89}Zr] Zr-oxalate solution 40–50 MBq (1–1.5 mCi) was added to nanoparticles, and the pH was adjusted to 7.0–7.5 with 2.0 M Na_2CO_3. The mixture was incubated at 37°C for 1 hour, resulting in the formation of ^{89}Zr-labeled lipoplex nanoparticles (^{89}Zr-LNP) (Figure 2).

The ^{89}Zr labeling of gemini surfactant was confirmed by RP-HPLC method with XBridge (Waters Corp., Milford, MA, USA) C18 analytical column (5 µm, 4.6×150 mm). Gradient elution was performed at a flow rate of 1 mL/min using a Waters 2796 HPLC System. Detection was performed using a Waters 2487 absorbance detector at 254 nm and using a Flow-Ram Radio-HPLC detector. The same condition was used as for the non-labeled surfactant. Briefly, the mobile phase consisted of 0.1% trifluoroacetic acid in H_2O (solution A) and 0.1% trifluoroacetic acid in acetonitrile (solution B). The mobile phase was programmed as follows: gradient from 90% A:10% B to 10% A:90% B in 30 minutes.

The radiochemical purity (RCP) of radiolabeled surfactant and lipoplex nanoparticles solutions was evaluated by instant thin layer chromatography (ITLC) also. Plates were developed in 20 mM sodium citrate (pH 5.5). The retention factor of labeled surfactant and lipoplex nanoparticles was <0.1; however, the retention factor of the free radio metal was >0.9.

$$\%\ \text{chelated}\ ^{89}\text{Zr} = \frac{\text{Counts from the strip at the origin}}{\text{Total counts on the strip}} \times 100$$

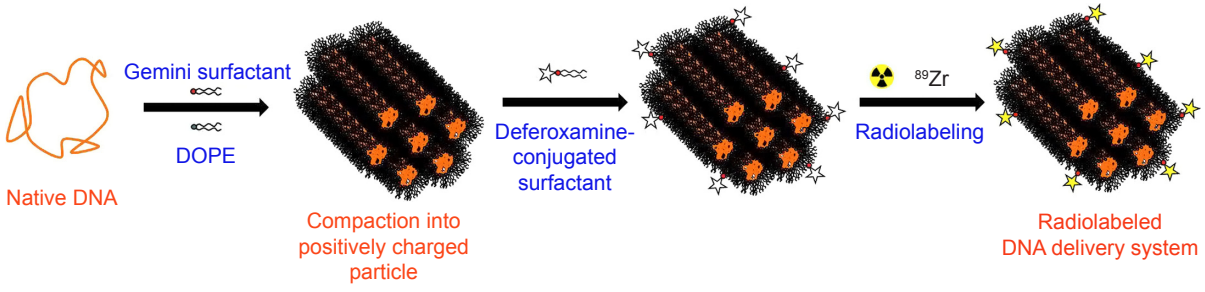

Figure 2 Schematic drawing of lipoplex assembly and radiolabeling procedures of the gene delivery nanosystem.
Abbreviation: DOPE, 1,2-dioleoyl-sn-glycero-3-phosphoethanolamine.

The distribution of radioactivity in developed ITLC plates was determined with the Automatic Wizard^2 Gamma Counter. HEPES-buffered ^{89}Zr-solution was used as a control. For stability studies, ^{89}Zr-labeled surfactant and ^{89}Zr-labeled lipoplex nanoparticles were added to 0.5 mL mouse serum and PBS in 1:10 volume ratio and incubated at 37°C for 72 hours. At 24 hours intervals, samples were taken from the solution and evaluated using ITLC and gamma counting.

Characterization of lipoplex nanoparticles

Size and zeta potential measurements

The hydrodynamic size, size distribution and zeta potential measurements were obtained by dynamic light scattering and laser Doppler micro-electrophoresis technique using a Malvern Zetasizer Nano ZS instrument (Malvern Instruments Ltd, Malvern, Worcestershire, UK). Particle size measurements were performed using a particle-sizing cell in the automatic mode. The mean hydrodynamic diameter was calculated from the autocorrelation function of the intensity of light scattered from the particles. Size distribution values were derived from three measurements, each consisting of a minimum of ten individual runs. The data are reported as intensity distribution. Zeta potential of the nanoparticles was determined by phase analysis light scattering analysis. Samples were measured in the automatic mode and the reported zeta potentials are the average of three measurements, each derived from a minimum of ten individual runs.

Transmission electron microscopy (TEM)

A HT7700 transmission electron microscope (Hitachi Corp, Tokyo, Japan) was used to characterize the morphology of the dried lipoplex nanoparticles. For TEM observation, the lipoplex nanoparticle formulations were prepared as for the in vitro and in vivo study. The samples for TEM analysis were obtained by placing a drop (10 µL) of lipoplex nanoparticles onto a formvar/carbon-coated copper grid. Excess liquid was wicked away with absorbent tissue after 2-minutes incubation and the grids were dried at room temperature. The grids were rinsed in water for 30 seconds then floated on a droplet of phosphotungstic acid for 1 minute for negative staining. The grids were rinsed and the thin layer was allowed to dry.

SAXS measurements

The formulations were prepared as for the transfection study using ten times higher concentrations. The SAXS experiments were performed at the BL4-2 beam line at Stanford Synchrotron Radiation Lightsource (SSRL, Stanford, CA, USA) using a wavelength of 1.1271 Å (11KeV energy). The scattered X-ray was detected on MAR225-HE (225×225 mm (3,072×3,072 pixels, pixel size 73.24 µm) at 20 seconds exposure time and at sample to detector distance of 1.1 m. The SAXS detector was calibrated with silver behenate. GSASII software was used to plot diffraction intensity vs 2θ (where θ is the diffraction angle) or the scattering vector ($q = \frac{4\pi}{\lambda}\sin\theta$) by radial integration of the two-dimensional patterns.

Characterization of ^{89}Zr-labeled gemini surfactant and nanoparticles

Cell line and animals

A375, human amelanotic melanoma cells (American Type Culture Collection CRL-1619), were used as a model for future development of image-guided therapy for melanoma and were purchased from Cedarlane (Burlington, ON, Canada). The cells were grown as monolayer cultures at 37°C in a humidified incubator with 5% CO_2 and 95% air and passaged in DMEM (Gibco) supplemented with 10% FBS (Gibco), 100 U/mL penicillin, 100 µg/mL streptomycin and 25 ng/mL amphotericin B (Sigma). For all experiments, passage numbers and incubation times were kept consistent. The cell culture was purchased from BD Biosciences. Female athymic CD-1 nude mice were purchased from Charles River Laboratories International, Inc. Animals were housed under pathogen-free conditions in air-conditioned rooms and artificial lighting with a circadian cycle of 12 hours. The diet and drinking water were available ad libitum to all the animals. This work was approved by the University of Saskatchewan Animal Research Ethics Board, and adhered to the Canadian Council on Animal Care guidelines for humane animal use (protocol Nos: 20130103 and 20150044).

Gene expression and cell proliferation assay

On the day before transfection, cells at the second passage were seeded at a density of 1×10^4 cells per well in 96-well tissue culture-treated plates (Falcon, BD Mississauga, ON, Canada) and then incubated at 37°C in a humidified incubator with 5% CO_2 and 95% air for 24 hours. One hour prior to treatment, the supplemented DMEM was replaced with DMEM. The cells were treated with standard nanoparticle formulation and the deferoxamine-modified nanoparticles formulations in 0.2 µg pGThCMV. IFN-GFP plasmid/well concentration (n=6 per treatment group). Lipofectamine Plus reagent (Invitrogen Life Technologies) was used as a positive control according to the manufacturer's protocol

in 0.2 μg pDNA/well concentration. Then the tissue culture plates were incubated in CO_2 incubator at 37°C for 5 hours when the transfection agents were removed and replaced with supplemented DMEM. Supernatants were replaced with fresh supplemented DMEM in every 24 hours and were collected with the secreted IFN-γ at the end of the experiment 72 hours after the transfection. The collected supernatants were stored at 80°C. For the quantification of the IFN-γ, ELISA was performed using flat bottom 96-well plates (Synergy HT, BioTek, Winooski, VT, USA) following the BD Pharmingen protocol as described earlier.[36] The concentration of expressed IFN-γ was calculated from a standard IFN-γ curve using recombinant mouse IFN-γ standard (BD Pharmingen, BD Biosciences). The cells treated with media were considered as negative control where the gene expression value is zero. For the cell proliferation experiment, fresh media containing a concentration of 450 μg/mL 3-(4,5-dimethylthiazol-2-yl)-2,5-diphenyltetrazolium bromide (MTT, Invitrogen) solution was added to each well, and the plates were incubated at 37°C for 2 hours. When purple precipitate was clearly visible under microscope, the MTT solution was removed and DMSO was added to each well, and the plates were incubated for 10 minutes at 37°C to dissolve the trapped formazan. Absorbance of the wells was measured at 550 nm using a Synergy HT BioTek plate reader. Proliferation of untreated cells was determined as a control.

Pharmacokinetic and biodistribution of ^{89}Zr-labeled gemini surfactant and nanoparticles

Normal athymic CD-1 mice (n=4 per group) were injected intravenously via the tail vein with 3–4 MBq ^{89}Zr-labeled surfactant or ^{89}Zr-labeled lipoplex nanoparticles. Blood samples (25–35 μL) were collected from the saphenous vein at a series of time points (5 minutes to 72 hours) into a capillary tube. The volume of the blood was determined by measuring the length of the blood sample in the capillary tube using a digital caliper. Thereafter, the capillary tube was moved to a γ-counting tube, and the radioactivity was measured in a γ-counter and expressed as a percentage of the injected activity per mL (% IA/mL). Pharmacokinetic parameters were calculated by fitting the blood radioactivity concentrations vs time to a two-compartment model using Prism 5.0 software (GraphPad). The half-life ($t_{1/2}$), area under the percentage of the injected activity per mL vs time curves (AUC), clearance (CL) and volume of distribution (Vd) were calculated. For biodistribution studies, the animals were euthanized under deep anesthesia and tissue samples including small intestine, stomach, lung, heart, muscle, liver, spleen and kidneys were harvested at 6, 24, 48 and 72 hours post injection. Samples of selected tissues were excised and weighed and the amounts of radioactivity in tissue samples were measured using an automatic γ-counter. For the calculation, the "time zero" (t_0) time point was used, representing the time of the injection, the decay corrected activity, and weight of selected tissues. The radioactivity in the organs was expressed as percent injected activity per gram (% IA/g).

PET imaging in tumor bearing mice

Athymic CD-1 mice bearing A375 xenografts (n=4 per group) were injected via a tail vein with 12–15 MBq of ^{89}Zr-labeled gemini surfactant or of ^{89}Zr-labeled nanoparticles. At 2, 24, 48 and 72 hours after injection, PET and CT images acquired in the MILabs Vector4CT scanner (Molecular Imaging Laboratories, MILabs B.V., Leiden, the Netherlands). PET scans were acquired in a list-mode data format with a high-energy ultra-high resolution (HE-UHR-1.0 mm) mouse/rat pinhole collimator. Corresponding CT scans were acquired with a tube setting of 50 kV and 480 μA. Images were reconstructed using a pixel-based order-subset expectation maximization algorithm that included resolution recovery and compensation for distance-dependent pinhole sensitivity and were registered on CT and quantified using PMOD 3.8 software (PMOD Technologies, Zürich, Switzerland). The scale was set at 2 hours and decay-corrected for subsequent time points. Tracer uptake was expressed as percentage injected activity (% IA) per cc of tissue volume (% IA/cc).

Statistical analyses

All characterization experiments were performed in triplicates at the minimum and the results are expressed as mean values ± SD. Statistical analyses were evaluated by ANOVA followed by the Bonferroni post hoc test using SPSS version 23.0 (IBM Corporation, Armonk, NY, USA). Significant differences were considered at $P<0.05$ values.

Results

Synthesis

In order to label the DNA delivery lipoplex nanoparticles with ^{89}Zr, 12-7NGK-12 gemini surfactant and deferoxamine-modified gemini surfactant were synthesized in seven steps. Following synthesis, both compounds were chemically characterized by HPLC (Figure S1), NMR (Figure S2A) and high-resolution MS. The theoretical and measured mass of synthesized compounds were in concordance

Table 1 Formulation and physicochemical properties of parent (LNP_0) and deferoxamine modified (LNP_2.5-LNP_10) lipoplex nanoparticles

Formulation ID	Size (nm)	PDI	Zeta potential (mV)
1: LNP_0 (0%)	115±5	0.168	29.5±0.7
2: LNP_2.5 (2.5%)	116±3	0.197	31.3±0.9
3: LNP_5 (5%)	116±2	0.172	33.1±0.7
4: LNP_7.5 (7.5%)	111±3	0.161	32.8±0.4
5: LNP_10 (10%)	114±4	0.170	31.3±0.3

Note: Size and zeta potential values represent the mean ± SD.
Abbreviation: PDI, polydispersity index.

where 6-((2-(bis(3-(dodecyldimethylammonio)propyl) amino)-2-oxoethyl)amino)-6-oxohexane-1,5-diaminium chloride, 12-7NGK-12 MS m/z: calculated mass: 355.3557, found mass: 355.3571 $[M]^{2+}/2$. *N*,*N*′-(((2-(2-amino-6-(3-(4-(3-(3,14,25-trihydroxy-2,10,13,21,24-pentaoxo-3,9,14,20-tetraazatriacontan-30-yl)thioureido)phenyl) thioureido)hexanamido)acetyl)azanediyl)bis(propane-3, 1-diyl))bis(*N*,*N*-dimethyldodecan-1-aminium) chloride, 12-7NGK-Deferoxamine-12, MS *m*/*z*: calculated mass: 731.5232, found mass: 731.5338 $[M]^{2+}/2$ (Figure S2B).

Formation and characterization of lipoplex nanoparticles

The non-modified lipoplexes had particle size of 115±5 nm and zeta potential of +29.5±0.7 mV. Adding deferoxamine-modified gemini surfactant to the lipoplexes did not change the size significantly, remaining in the range of 111–117 nm. The polydispersity index also remained under 0.2. The zeta potential increased slightly from 29.5±0.7 to 31–33 mV. There was no significant difference ($P>0.05$) in the particle size and zeta potential values between the non-modified and deferoxamine-modified lipoplexes (Table 1). Particle morphology and aggregation behavior can also influence the in vitro and in vivo behavior of nanoparticles. The TEM images of the non-modified and deferoxamine-modified lipoplex nanoparticles showed consistency with the previous light scattering measurement and showed no aggregation behavior of the particles (Figure 3). SAXS data demonstrated that an inverted hexagonal phase was adopted in both modified and non-modified lipoplexes (Figure 4). The position of the scattering peaks and the corresponding unit cell spacing ($a=4\pi/\sqrt{3}\ q_{10}$) (where q_{10} is the first Bragg peak) were at q_{10}=0.097, q_{11}=0.167 and q_{20}=0.193 corresponding to the inverted hexagonal structure with the ratio of $1:\sqrt{3}:\sqrt{4}$[40] and a unit cell spacing a=74.796 Å for the deferoxamine-modified lipoplexes, similar to the non-modified lipoplexes at q_{10}=0.098, q_{11}=0.168 and q_{20}=0.195 corresponding to a unit cell spacing a=74.033 Å. Thus, modification with deferoxamine did not change the overall gemini surfactant organization in the nanoparticles significantly, as we expected.

^{89}Zr labeling and stability of gemini surfactants and nanoparticles

On the basis of the ITLC and the HPLC results (Figure S3), the labeling efficiency in case of ^{89}Zr-labeled surfactant was greater than 95% (98.6%±2.4% ITLC, 96.5%±1.3% HPLC) and in case of ^{89}Zr-labeled lipoplex nanoparticles was 95.2%±3.4%; therefore, further purification of the complexes was not necessary.

Under the same reaction conditions, labeling efficiency was not detectable by non-modified gemini surfactant and non-modified nanoparticles. The maximum specific activity of the deferoxamine-modified gemini surfactant was 5 MBq/μg. Specific activity of the 2.5%, 5%, 7.5% and 10% deferoxamine-modified nanoparticles was 19.7±3.5 MBq/mg, 34.4±5.5 MBq/mg 54.8±3.8 MBq/mg and 78.8±9.4 MBq/mg, respectively.

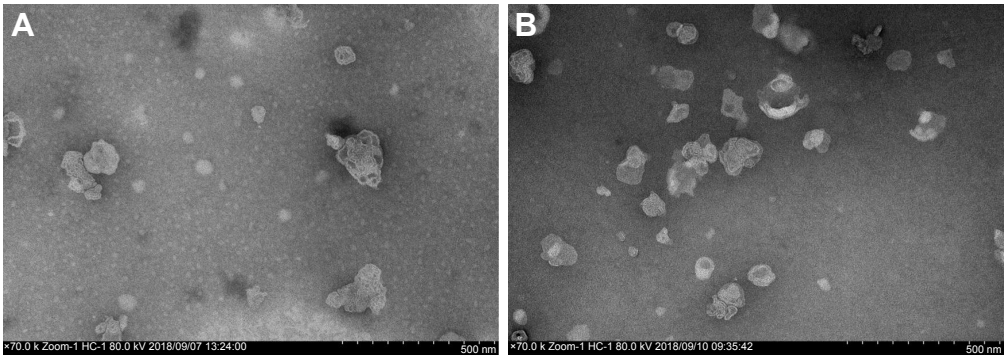

Figure 3 TEM images of (**A**) non-modified and (**B**) deferoxamine-modified lipoplex nanoparticles (LNP).

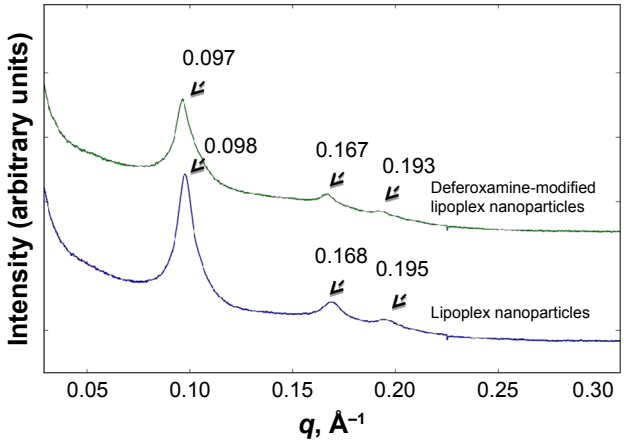

Figure 4 SAXS scattering profile of deferoxamine-modified and non-modified lipoplex nanoparticles (LNP).

The dissociation of ^{89}Zr from radiolabeled gemini surfactants and nanoparticles in mouse serum and PBS was evaluated by ITLC. Over a 72 hour period, there was no significant loss of ^{89}Zr (formation of free ^{89}Zr) from ^{89}Zr-labeled surfactant and ^{89}Zr-labeled lipoplex nanoparticles in serum or PBS. In both serum and PBS, the RCP of ^{89}Zr-labeled surfactant decreased from 95.2%±3.4%–94.2%±2.9% in mouse serum and to 92.6%±3.3% in PBS. Similarly, the RCP of ^{89}Zr-labeled lipoplex nanoparticles decreased from 95.26% to 94.21% and 92.64% in serum and PBS, respectively (Figure 5).

Determination of gene expression and cell viability

The influence of the amount of modified gemini surfactants in nanoparticle formulation on the gene expression and cell viability was investigated in A375 humane melanoma cells. The level of expressed IFN-γ in case of non-modified nanoparticles was the highest of 1,202±148 pg/10^3 cells. The modified formulations showed slightly lower efficiency of 925±116 pg, 944±352 pg, 936±158 pg and 896±280 pg of IFN-γ/10^3 A375 cells for the 2.5%, 5%, 7.5% and 10% replacement with modified gemini surfactants, respectively (Figure 6A). However, no significant difference ($P<0.05$) between the transfection efficiency of the standard non-modified and deferoxamine-modified formulations was observed. The viability of A375 cells treated with non-modified nanoparticle was 83%±18% of the non-treated cells (Figure 6B). Incorporation of 2.5%–10% deferoxamine-modified gemini

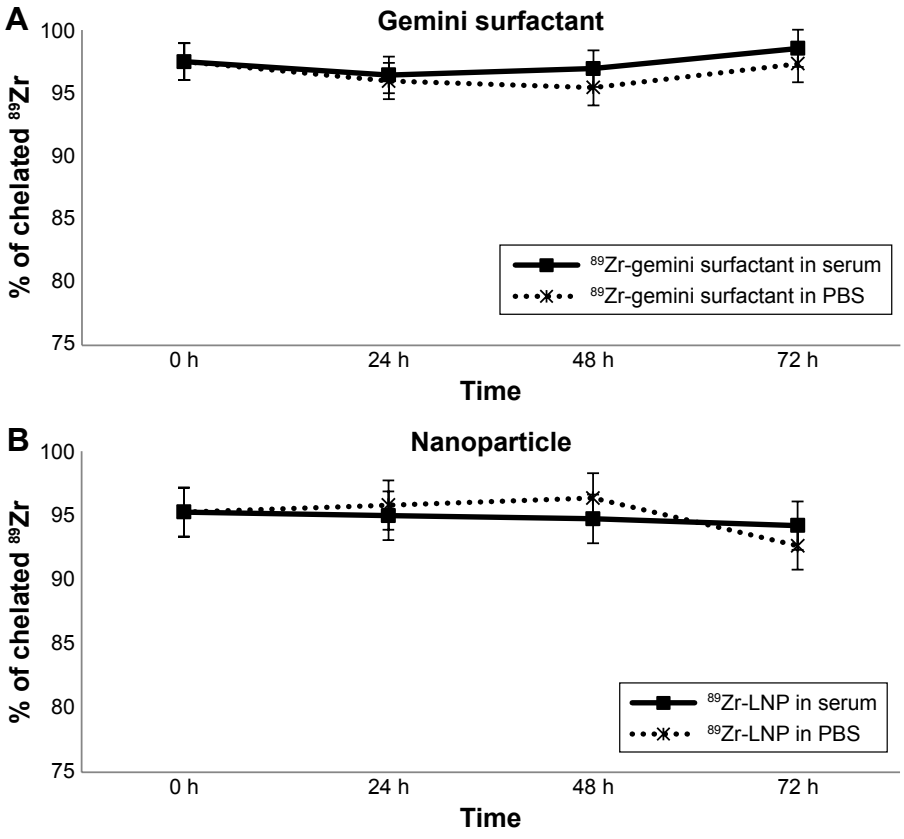

Figure 5 Stability testing of ^{89}Zr-labeled gemini surfactant (**A**) and ^{89}Zr-labeled lipoplex nanoparticles (LNP) (**B**) in mouse serum and PBS during the 72 hours at 37°C.
Note: Error bars present SD, n=4.

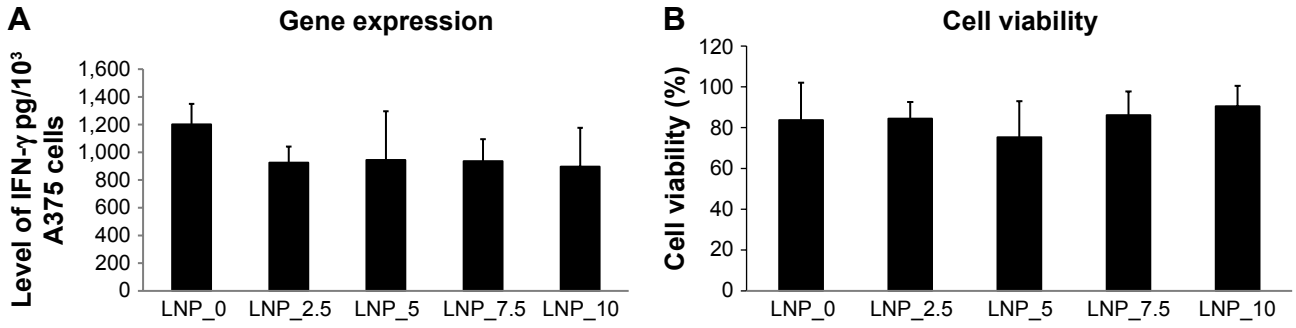

Figure 6 Gene expression (**A**) and cell viability (**B**) of A375 cells treated with non-modified and deferoxamine-modified lipoplex nanoparticles (LNP).
Note: Error bars present SD, n=6 per treatment group.

surfactant did not alter cell viability, remaining in the acceptable range of 84%–89%, indicating no significant change between the cell viability of non-modified and deferoxamine-modified nanoparticle formulations.

Pharmacokinetics and biodistribution

Pharmacokinetics of ^{89}Zr-labeled gemini surfactant and ^{89}Zr-labeled lipoplex nanoparticles was studied in healthy athymic CD-1 nude mice. There was an overall significant difference ($P<0.05$) in the pharmacokinetic parameters of the ^{89}Zr-labeled nanoparticles. Notably, the half-life of the nanoparticles ($t_{1/2}$=10.1±0.4 hours) was significantly higher compared with the ^{89}Zr-labeled surfactant ($t_{1/2}$=1.3±0.1 hours). Similarly, the AUC was significantly larger for the nanoparticles (AUC =561%±135% IA/mL×hours) vs the labeled surfactant (AUC =148%±87% IA/mL×hours). Conversely, the Vd of the surfactant alone (Vd =39.3±12.3 mL) was larger compared with the lipoplexes (Vd =2.0±0.7 mL), while the CL of ^{89}Zr-labeled lipoplex of CL =0.18±0.04 mL/h was markedly lower compared with the ^{89}Zr-labeled surfactant of CL =1.23±0.85 mL/h (Figure 7, Table 2).

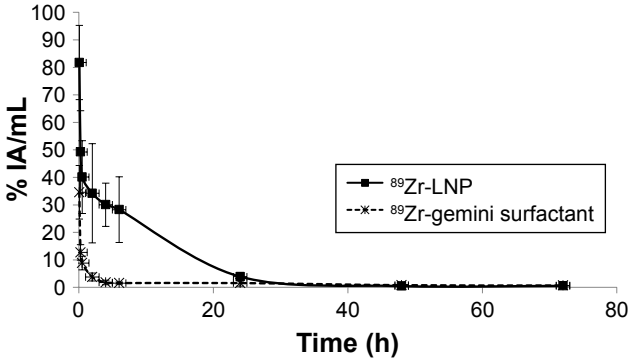

Figure 7 Blood clearance of ^{89}Zr-labeled surfactant and ^{89}Zr-labeled lipoplex nanoparticles (LNP) in healthy athymic CD-1 nude mice.
Note: Error bars present SD, n=4 per group.

Furthermore, quantitative whole organ biodistribution data obtained from automatic γ-counter analysis are shown in Table 3. The highest accumulation of radiolabeled nanoparticles was found in the liver (33.87%±2.20% IA/g) and spleen (24.76±11.34) at 72 hours post injection. The liver accumulation of ^{89}Zr-LNP was 5.49±1.29, 21.59±1.95, 19.40±4.87 and 33.87%±2.20% IA/g the spleen accumulation of ^{89}Zr-LNP was 6.59±0.96, 9.01±0.42, 14.76±1.52 and 24.76%±11.34% IA/g at 6, 24, 48 and 72 hours post injection, respectively. The liver and the spleen uptake showed similar increasing trend from 6 to 72 hours post injection. The ^{89}Zr-LNP accumulation in the additional specified organs was under 5% IA/g and showed decreasing trend during the 72 hours. The highest accumulation was found in the liver (20.75%±5.35% IA/g at 72 hours) and spleen (29.54%±2.41% IA/g at 6 hours) also in case of radiolabeled surfactant; however, there was no trend and significant differences in the liver and spleen uptake through the 72 hours post injection. The kidney uptake of ^{89}Zr-Surfactant was 2.42±0.23, 1.86±0.22, 1.87±0.20 and 1.34%±0.16% IA/g and statistically significantly higher ($P<0.05$) than the ^{89}Zr-LNP at 6, 24, 48 and 72 hours post injection, respectively.

PET imaging and tumor accumulation

PET imaging shows similar pattern to the biodistribution studies assessed by gamma counting (Figure 8). ^{89}Zr-labeled gemini surfactant shows early accumulation in the kidneys and bladder (Figure 8A), while there is a more diffuse distribution of the radiotracer in the animals treated with ^{89}Zr-labeled lipoplex nanoparticles at 2 hours (Figure 8B). At later time points (24–72 hour), both gemini surfactant and lipoplex nanoparticles show accumulation in the liver. Tumor uptake (Figure 8, areas marked by red circles on the tomographs) of the lipoplexes was higher compared with

Table 2 Pharmacokinetic parameters of ^{89}Zr-labeled LNP and ^{89}Zr-labeled gemini surfactant

Formulation ID	$t_{1/2}$ (h)	AUC (% IA/mL X h)	Vd (mL)	CL (mL/h)
^{89}Zr-LNP	10.1±0.4	561±135	2.0±0.7	0.18±0.04
^{89}Zr-gemini surfactant	1.3±0.1	148±87	39.3±12.3	1.23±0.85

Abbreviations: AUC, area under the curve; CL, clearance; LNP, lipoplex nanoparticles.

the gemini surfactant. Quantitatively, tumor uptake was determined using PMOD software (Figure 9). At 2 hours post injection, tumor uptake was significantly higher ($P<0.05$) for the ^{89}Zr-lipoplex nanoparticles (3.48% IA/cc) compared with the gemini surfactant (2.08% IA/cc). At later time points, tumor uptake of ^{89}Zr-lipoplex nanoparticles remained higher than for ^{89}Zr-gemini surfactant even though the difference was not significant.

Discussion

In this present study, we have modified our gemini surfactant-based DNA delivery nanoparticles with deferoxamine to chelate ^{89}Zr for PET imaging. We selected deferoxamine as previous studies showed that labeling nanoparticles and antibodies with ^{89}Zr could be effectively performed with high specific activity using this chelator.[41] Seo et al initially introduced ^{89}Zr labeling with deferoxamine, which forms a thiourea during the coupling reaction.[23] In our case, deferoxamine was conjugated to a primary amine of the 12-7NGK-12 surfactant using conventional conjugation protocol at pH 8.5.[42] The specific chemical properties of the deferoxamine and primary amines on the gemini surfactants makes this conjugation a robust and reproducible methodology. This successful conjugation will be the basis of future labeling of gemini surfactants and could be expanded to other similar cationic surfactants in order to create a tool for monitoring their biodistribution by PET.

We demonstrated in earlier studies that substitutions on the gemini surfactants modified their physicochemical properties (eg, particle size, zeta potential and critical micellar concentration) compared with the first-generation gemini surfactants, and led to a significant increase in their biological effect, namely gene expression efficiency, without increase in toxicity.[32,35] As the deferoxamine might also affect the assembly of the nanoparticles, we compared the behavior of the original parent nanoparticles with the newly created deferoxamine-modified nanoparticles aiming for conservation of their properties after modification. We did not find significant size difference between the non-modified and deferoxamine-modified lipoplex nanoparticle formulations (Table 1). The ratio of deferoxamine-modified gemini surfactants did not change the hydrodynamic size of lipoplex particles. The average size of all formulations remained 100–120 nm, optimal for endocytotic internalization by the cells.[43] There was no difference between the zeta potential of the non-modified and deferoxamine-modified nanoparticles, indicating that modification did not affect the positive surface charge on the particles that is necessary for the interaction with the negatively charged surface of mammalian cells facilitating endocytosis.[44] The values of approximately +30 mV also indicates that both non-modified and deferoxamine-modified systems are colloidally stable, an important factor in pharmaceutical formulation development.[45] Electron microscopy images also support the uniform mono-modal particle

Table 3 Normal tissue uptake in healthy athymic CD-1 nude mice 6, 24, 48 and 72 hours after intravenous injection

Tissue	^{89}Zr-lipoplex nanoparticles (LNP)				^{89}Zr-gemini surfactant			
	6 hours	24 hours	48 hours	72 hours	6 hours	24 hours	48 hours	72 hours
Small intestine	1.31±0.36	0.32±0.05	0.32±0.14	0.14±0.03	0.35±0.10	0.17±0.02	0.13±0.02	0.12±0.03
Heart	1.85±0.22	0.97±0.20	0.63±0.12	0.31±0.08	0.25±0.08	0.18±0.04	0.16±0.02	0.10±0.03
Kidney	1.56±0.27	1.63±0.31	1.51±0.37	0.95±0.08	2.42±0.23	1.86±0.22	1.87±0.20	1.34±0.16
Liver	5.49±1.29	21.59±1.95	19.40±4.87	33.87±2.20	19.99±0.54	14.76±2.99	15.88±1.89	20.75±5.34
Lung	2.80±0.50	4.52±0.89	2.67±0.93	1.07±0.07	3.22±1.24	1.69±0.75	2.17±1.46	0.94±0.36
Muscle	0.78±0.23	0.36±0.14	0.18±0.04	0.21±0.01	0.16±0.01	0.08±0.01	0.08±0.01	0.08±0.02
Spleen	6.59±0.96	9.01±0.41	14.76±1.52	24.76±11.34	29.54±2.41	25.00±4.44	29.28±5.67	23.83±12.26
Stomach	0.79±0.25	0.26±0.04	0.15±0.05	0.18±0.03	0.18±0.03	0.07±0.04	0.05±0.03	0.07±0.02

Note: Unit is % IA/g.

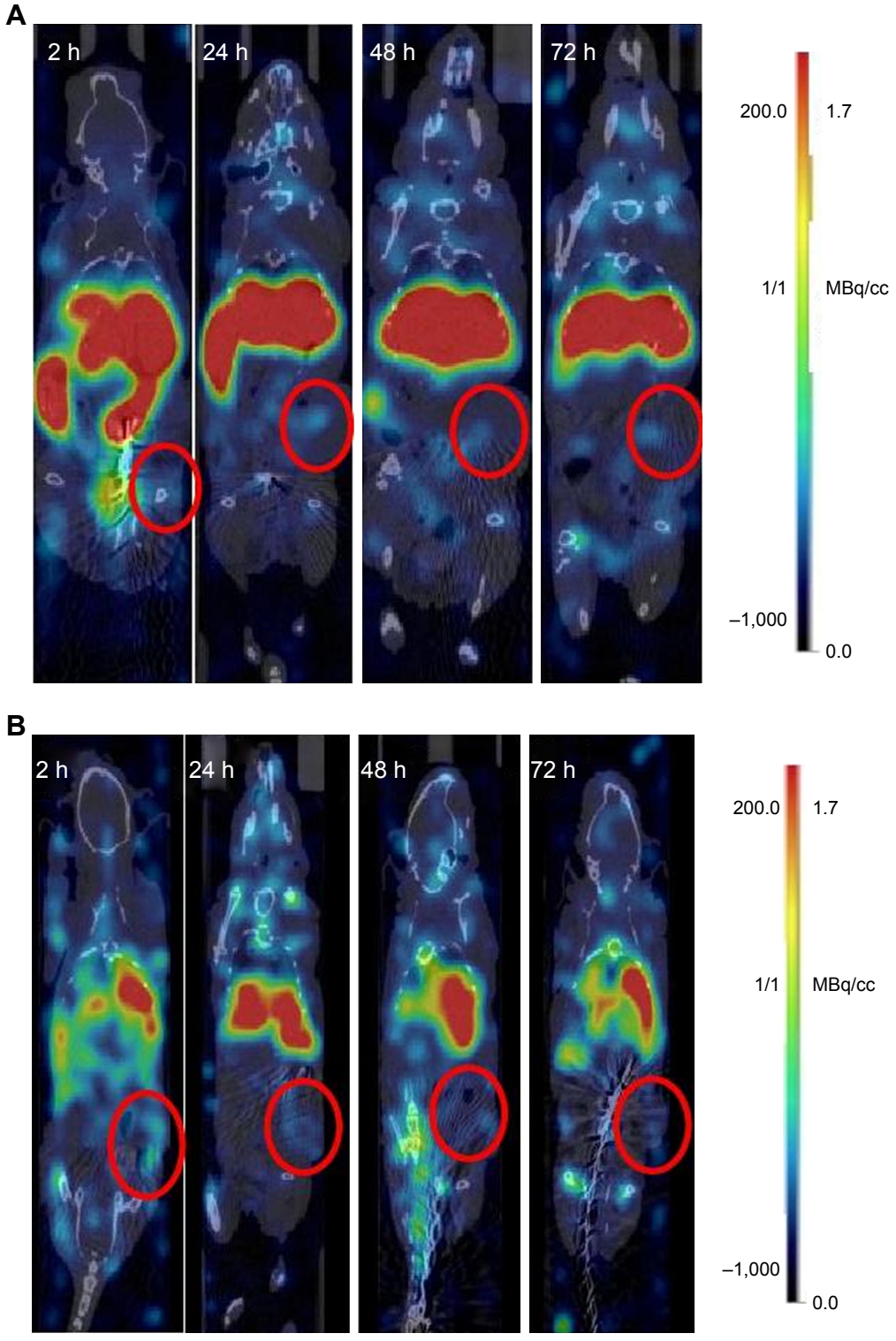

Figure 8 Positron-emission tomographs of representative animals at 2, 24, 48 and 72 hours post injection of (**A**) ^{89}Zr-gemini surfactant and (**B**) ^{89}Zr-lipoplex nanoparticles (LNP) tumor position was identified on the computed tompgraphic scan and red circles indicate the area of the tumor.

distribution (ie, no aggregation of the nanoparticles) and the similar morphology of the non-modified and deferoxamine-modified lipoplexes (Figure 3). The inverted hexagonal phase is known to be responsible for high transfection efficiency of lipid-based nanoparticles due to the ability of this kind of assembly to facilitate the fusion of the nanoparticles with the cell membrane and cytoplasmic release of the DNA into the cytosol.[46] Recently, we demonstrated that the shape of

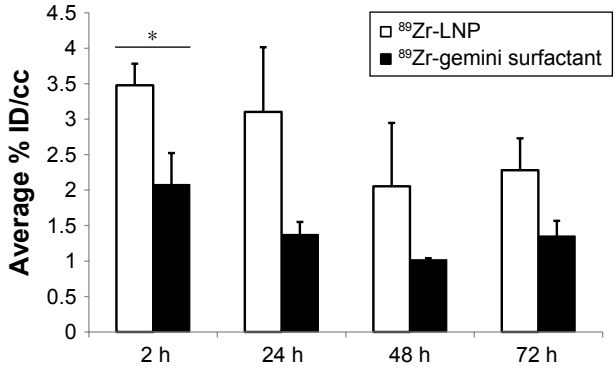

Figure 9 Tumor accumulation of the ^{89}Zr-gemini surfactant and ^{89}Zr-lipoplex nanoparticles (LNP) by microPET/CT.
Notes: The values for % IA/cc are decay-corrected from PET/computed tomographic images. Error bars present SD, n=4 per group. *$P<0.05$.

the gemini surfactant molecule plays an important role in the overall structural organization of the nanoparticles in the presence of helper lipid DOPE. Variations between the ratios of the hydrophilic headgroup and hydrophobic tail area of the gemini surfactants can lead to changes in structural organization, a factor that, in our estimation, is critical, a determinant of the transfection efficiency.[47] Thus, for this study, it was important to ascertain that this structural organization is maintained after modification of the nanoparticles.

In addition to the stability of the nanoparticles formulated with deferoxamine-modified surfactants, the complexation with the radioactive element, ^{89}Zr might also pose challenges. Using the isotonic condition during ^{89}Zr complexation was important to retain the stability of the nanoparticles. This procedure resulted in a stable and highly efficient labeling for both deferoxamine-modified surfactants and deferoxamine-modified nanoparticles, similar to other ^{89}Zr complexation studies.[42,48] Thus, this labeling strategy is suitable for performing further in vitro and in vivo investigations.

While there are several in vitro stability tests of ^{89}Zr-labeled monoclonal antibodies and nanoparticles in the literature, there are no reports to our knowledge on labeling and using cationic gemini surfactants. Perk et al investigated the stability of ^{89}Zr-labeled monoclonal antibodies (^{89}Zr-deferoxamine-mAbs) in serum at 37°C. It was found that the loss of ^{89}Zr from ^{89}Zr-deferoxamine-mAbs was less than 4% at 72 hours and was less than 4.7% after a 7-day incubation period.[42] Keliher et al tested ^{89}Zr-labeled dextran nanoparticles (^{89}Zr-DNPs) and found that the nanoparticles did not show any sign of degradation at 36°C in PBS.[49] Furthermore, stability of ^{89}Zr-labeled liposome was evaluated in serum at 37°C for 48 hours by Seo et al.[23] The results showed less than 3% loss of ^{89}Zr over the 48 hours. Using similar experimental design, we monitored the stability of the ^{89}Zr-labeled surfactant and ^{89}Zr-labeled nanoparticles for 72 hours in order to match the timeframe with the hypothesized residence of the nanoparticles in the body. Our stability tests for the gemini surfactants showed promising outcome as there was no ^{89}Zr loss during the 72 hours evaluation in mouse serum and PBS. The nanoparticles stability showed a minimal loss of ^{89}Zr from the lipoplexes. The ^{89}Zr loss from nanoparticles was less than 3% from PBS and even lower at 2% from biologically relevant medium, mouse serum (Figure 5). These results demonstrate that the self-assembling gemini nanoparticles are stable complexes and do not lose their structural integrity in the presence of serum, an important factor to consider for intravenous administration. As mentioned earlier, modification of the structure could lead to the alteration of the biological activity and safety of the lipoplex nanoparticles. The deferoxamine-modifications did not cause significant changes in the biological activity, as observed by the levels of gene expression, and cell viability, compared with the non-modified nanoparticles (Figure 6). We hypothesized that the similarity in the physicochemical properties and in vitro efficiency and toxicity between the deferoxamine-modified and parent nanoparticles gives us a good prediction that their in vivo behavior will also be similar.

For diagnostic and image-guided drug delivery applications, it is necessary that the nanoparticles are stable in vivo and the radiolabels remain associated with the nanoparticles in the circulation. Here, we investigated the pharmacokinetics parameters and biodistribution of ^{89}Zr-labeled gemini surfactant and ^{89}Zr-labeled nanoparticles after intravenous injection to mice. The differences in pharmacokinetic parameters were as expected: the ^{89}Zr-labeled nanoparticles had a higher plasma half-life and lower CL compared with the ^{89}Zr-labeled surfactant (Figure 7, Table 2), namely, a sevenfold lower plasma half-life and expressively higher CL. Wang et al investigated the pharmacokinetics of ^{111}In/^{177}Lu-liposome in BALB/c mice. It was found that the half-lives of 100 nm sized ^{111}In- and ^{177}Lu-liposomes in blood were 10.2 and 11.5 hours, respectively.[50] Seo et al evaluated the CL of ^{89}Zr-labeled liposomes with a size of 120 nm from blood, and the image-based pharmacokinetic study showed the half-life of ^{89}Zr-labeled liposomes was 13.3 hours.[23] The 10-hour plasma half-life of the gemini nanoparticles indicates that nanoparticles remained intact in the blood. This long circulation time permits these nanoparticles to spend sufficient time in the blood stream to accumulate in the tumor.[51]

In addition to the blood CL, the biodistribution data were also investigated. Several biodistribution studies of radiolabeled liposomes can be found in the recent literature.

However, there are few studies with ^{89}Zr-labeled nanoparticles and no studies on gemini surfactants. Kang et al evaluated the biodistribution of ^{64}Cu-labeled liposomes in mice. MicroPET imaging and ex vivo tissue distribution analyses showed high radioactivity accumulation in the liver and spleen.[52] van der Geest et al found that the highest accumulation of the ^{111}In-labeled liposome was in the liver and spleen[53] and Seo et al also found that the higher residual radioactivity of the ^{89}Zr-labeled liposome was in the spleen and liver.[23] Similar to the liposomes, the ^{89}Zr-labeled gemini surfactant-based lipoplex nanoparticles also accumulated in spleen and liver. The uptake of the nanoparticles in the liver and the spleen showed increasing tendency from 6 to 72 hours post injection compared with the other organs, which showed decreasing trend in nanoparticles uptake. For ^{89}Zr-labeled surfactant, the liver and the spleen initially displayed a relatively high accumulation at 6 hours post injection with minimal changes through 72 hours post injection. On the basis of the images, the ^{89}Zr-labeled lipoplex nanoparticles exhibited an overall lower accumulation in the liver compared with the ^{89}Zr-labeled surfactant, which might be an advantage of the lipid-based nanoparticles. These outcomes support the pharmacokinetic data, namely that the ^{89}Zr-labeled lipoplex nanoparticles spend long time in the blood while the ^{89}Zr-labeled surfactant eliminate fast from the blood compartment (Table 3). The reason for the high nanoparticle uptake in the liver and spleen is that the liver and the spleen play a central role in the removal of foreign particles from the circulation, mainly via Kupffer cells and spleen macrophages.[54–56] The hepatobiliary system of the liver represents the primary route of excretion for particles. Furthermore, spleen macrophages are also activated in addition to liver Kupffer cells. Conversely, small molecules are cleared from the body through the kidney as we observed in the case of our gemini surfactants.[55] The fact that nanoparticles showed significantly higher liver accumulation, while the free surfactant showed higher kidney accumulation suggests that gemini surfactant and the nanoparticles had different route of metabolism. The low-level ^{89}Zr-labeled nanoparticles in the lung indicate that the nanoparticles remained dispersed and not aggregated in the blood. When the size of the injected nanoparticles is larger than 1 μm or the size of the injected nanoparticles increases to this value after the injection, high lung accumulation can be seen.[57,58] Furthermore, the absence of a bimodal CL (ie, fast CL of the gemini surfactants released from the nanoparticles followed by the second CL peak of the intact nanoparticles) also indicates that the nanoparticles do not disintegrate in the blood. While the concept of enhanced tumor uptake of non-targeted nanoparticles, attributed to the EPR effect, is controversial and amounts to less than 1% of the administered dose were taken by the tumor,[59] our nanoparticles showed a 3% tumor accumulation as early as 2 hours after administration. Similar tumor localization was found by Lee et al when chemotherapeutic drugs were encapsulated in liposomal delivery systems.[60]

Similarly, porphyrin-based liposomes showed 4%–7% ID/cc tumor uptake, depending on the type of cells injected to generate the orthotropic cancer model.[61] Nevertheless, these findings are the basis of further development and optimization of gemini surfactant-based gene delivery nanoparticles for cancer therapy. As conjugation of targeting vectors might improve accumulation of the nanoparticles in tumors, our next efforts focus on evaluation of targeted lipoplexes. The structural versatility of the gemini surfactants provided us with the opportunity to chemically attach peptides that target overexpressed surface ligands on melanoma cells. We found that incorporation of 10% of peptide-conjugated gemini surfactants into the nanoparticle formulation (similar to the formulation used in this study) improved reporter gene expression significantly.[62]

Conclusion

In this study, ^{89}Zr-labeled lipoplex nanoparticles were successfully produced and tested in vitro and in vivo. We identified that the replacement of the peptide-modified gemini surfactant with the deferoxamine-modified surfactant did not influence the physicochemical properties and biological activity of the gene delivery nanosystems. We demonstrated that the nanoparticles spend sufficient time in the blood stream, thus might promote tumor accumulation in cancer models. Future studies in tumor-bearing animals will probe this hypothesis. The lipoplex nanoparticles maintain structural integrity without shedding the radioactive label of gemini surfactants and their pharmacokinetic profile renders them applicable as potential theranostic or image-guided therapeutic agents. Our ability to monitor the tumor uptake of the nanoparticles in real time using PET imaging will increase our capacity to screen and optimize the gemini surfactant-based gene delivery nanoparticles. Overall, the outcome of our study indicates that ^{89}Zr-labeled DNA delivery nanosystems could become an attractive nanoplatform for cancer diagnosis and therapy.

Ethical conduct of research

The authors state that they have obtained appropriate institutional review board approval or have followed the

principles outlined in the Declaration of Helsinki for all human or animal experimental investigations.

Acknowledgments

This work and the stipend for Dr Hajdu were supported by grants from the Sylvia Fedoruk Canadian Centre for Nuclear innovation and the Natural Sciences and Engineering Research Council of Canada. We thank Waleed Mohammed-Saeid and Kevin Allen from the College of Pharmacy and Nutrition and Rufael Chekol from the College of Medicine for their assistance with chemical syntheses, formulation development and animal studies. We thank research staff at the Saskatchewan Centre for Cyclotron Sciences – Nuclear Imaging Facility for their assistance with imaging studies. Special thanks to Dr Elahe Alizadeh for assistance with the imaging software. We acknowledge Dr Jane Alcorn for assistance with the Prism software. The SAXS work was carried out at the Stanford Synchrotron Radiation Lightsource (SSRL), a Directorate of SLAC National Accelerator Laboratory, and an Office of Science User Facility operated for the US Department of Energy (DOE) Office of Science by Stanford University. The SSRL Structural Molecular Biology Program is supported by the DOE Office of Biological and Environmental Research, the National Institutes of Health (NIH), and the National Institute of General Medical Sciences (NIGMS; including P41GM103393). The contents of this publication are solely the responsibility of the authors and do not necessarily represent the official views of NIGMS or NIH. We acknowledge the assistance of Dr Thomas Weiss, SSRL, with instrument setting and data collection.

Disclosure

The authors report no conflicts of interest in this work.

References

1. Parveen S, Misra R, Sahoo SK. Nanoparticles: a boon to drug delivery, therapeutics, diagnostics and imaging. *Nanomedicine*. 2012;8(2):147–166.
2. Toy R, Bauer L, Hoimes C, Ghaghada KB, Karathanasis E. Targeted nanotechnology for cancer imaging. *Adv Drug Deliv Rev*. 2014;76:79–97.
3. Ma X, Zhao Y, Liang XJ. Theranostic nanoparticles engineered for clinic and pharmaceutics. *Acc Chem Res*. 2011;44(10):1114–1122.
4. Davis ME. The first targeted delivery of siRNA in humans via a self-assembling, cyclodextrin polymer-based nanoparticle: from concept to clinic. *Mol Pharm*. 2009;6(3):659–668.
5. Sankhala K, Mita A, Adinin R. A phase I pharmacokinetic (PK) study of MBP-426, a novel liposome encapsulated oxaliplatin. *J Clin Oncol*. 2009;27(15S):2535.
6. Li J, Wang Y, Liang R, et al. Recent advances in targeted nanoparticles drug delivery to melanoma. *Nanomedicine*. 2015;11(3):769–794.
7. Koo H, Huh MS, Sun IC, et al. In vivo targeted delivery of nanoparticles for theranosis. *Acc Chem Res*. 2011;44(10):1018–1028.
8. Shi J, Xiao Z, Kamaly N, Farokhzad OC. Self-assembled targeted nanoparticles: evolution of technologies and bench to bedside translation. *Acc Chem Res*. 2011;44(10):1123–1134.
9. Allen TM, Cullis PR. Liposomal drug delivery systems: from concept to clinical applications. *Adv Drug Deliv Rev*. 2013;65(1):36–48.
10. Al-Jamal WT, Kostarelos K. Liposomes: from a clinically established drug delivery system to a nanoparticle platform for theranostic nanomedicine. *Acc Chem Res*. 2011;44(10):1094–1104.
11. Al-Ahmady Z, Kostarelos K. Chemical components for the design of temperature-responsive vesicles as cancer therapeutics. *Chem Rev*. 2016;116(6):3883–3918.
12. Ravar F, Saadat E, Gholami M, et al. Hyaluronic acid-coated liposomes for targeted delivery of paclitaxel, in-vitro characterization and in-vivo evaluation. *J Control Release*. 2016;229:10–22.
13. Kunjachan S, Ehling J, Storm G, Kiessling F, Lammers T. Noninvasive imaging of nanomedicines and nanotheranostics: principles, progress, and prospects. *Chem Rev*. 2015;115(19):10907–10937.
14. Ryu JH, Lee S, Son S, et al. Theranostic nanoparticles for future personalized medicine. *J Control Release*. 2014;190:477–484.
15. Jokerst JV, Gambhir SS. Molecular imaging with theranostic nanoparticles. *Acc Chem Res*. 2011;44(10):1050–1060.
16. Chen F, Hong H, Zhang Y, et al. In vivo tumor targeting and image-guided drug delivery with antibody-conjugated, radiolabeled mesoporous silica nanoparticles. *ACS Nano*. 2013;7(10):9027–9039.
17. de Barros AB, Tsourkas A, Saboury B, Cardoso VN, Alavi A. Emerging role of radiolabeled nanoparticles as an effective diagnostic technique. *EJNMMI Res*. 2012;2(1):39.
18. Liu Y, Welch MJ. Nanoparticles labeled with positron emitting nuclides: advantages, methods, and applications. *Bioconjug Chem*. 2012;23(4):671–682.
19. Hamoudeh M, Kamleh MA, Diab R, Fessi H. Radionuclides delivery systems for nuclear imaging and radiotherapy of cancer. *Adv Drug Deliv Rev*. 2008;60(12):1329–1346.
20. Petersen AL, Hansen AE, Gabizon A, Andresen TL. Liposome imaging agents in personalized medicine. *Adv Drug Deliv Rev*. 2012;64(13):1417–1435.
21. Seo JW, Zhang H, Kukis DL, Meares CF, Ferrara KW. A novel method to label preformed liposomes with 64Cu for positron emission tomography (PET) imaging. *Bioconjug Chem*. 2008;19(12):2577–2584.
22. Li S, Goins B, Zhang L, Bao A. Novel multifunctional theranostic liposome drug delivery system: construction, characterization, and multimodality MR, near-infrared fluorescent, and nuclear imaging. *Bioconjug Chem*. 2012;23(6):1322–1332.
23. Seo JW, Mahakian LM, Tam S, et al. The pharmacokinetics of Zr-89 labeled liposomes over extended periods in a murine tumor model. *Nucl Med Biol*. 2015;42(2):155–163.
24. Abou DS, Thorek DL, Ramos NN, et al. ^{89}Zr-labeled paramagnetic octreotide-liposomes for PET-MR imaging of cancer. *Pharm Res*. 2013;30(3):878–888.
25. Nayerossadat N, Maedeh T, Ali PA. Viral and nonviral delivery systems for gene delivery. *Adv Biomed Res*. 2012;1:27.
26. Koide H, Okamoto A, Tsuchida H, et al. One-step encapsulation of siRNA between lipid-layers of multi-layer polycation liposomes by lipoplex freeze-thawing. *J Control Release*. 2016;228:1–8.
27. Dass CR. Biochemical and biophysical characteristics of lipoplexes pertinent to solid tumour gene therapy. *Int J Pharm*. 2002;241(1):1–25.
28. Dass CR, Choong PF. Selective gene delivery for cancer therapy using cationic liposomes: in vivo proof of applicability. *J Control Release*. 2006;113(2):155–163.
29. Duarte S, Faneca H, Lima MC. Folate-associated lipoplexes mediate efficient gene delivery and potent antitumoral activity in vitro and in vivo. *Int J Pharm*. 2012;423(2):365–377.
30. Tagami T, Suzuki T, Matsunaga M, et al. Anti-angiogenic therapy via cationic liposome-mediated systemic siRNA delivery. *Int J Pharm*. 2012;422(1–2):280–289.

31. He ZY, Wei XW, Luo M, et al. Folate-linked lipoplexes for short hairpin RNA targeting claudin-3 delivery in ovarian cancer xenografts. *J Control Release*. 2013;172(3):679–689.
32. Badea I, Verrall R, Baca-Estrada M, et al. In vivo cutaneous interferon-gamma gene delivery using novel dicationic (gemini) surfactant-plasmid complexes. *J Gene Med*. 2005;7(9):1200–1214.
33. Wettig SD, Wang C, Verrall RE, Foldvari M. Thermodynamic and aggregation properties of aza- and imino-substituted gemini surfactants designed for gene delivery. *Phys Chem Chem Phys*. 2007;9(7):871–877.
34. Wettig SD, Badea I, Donkuru M, Verrall RE, Foldvari M. Structural and transfection properties of amine-substituted gemini surfactant-based nanoparticles. *J Gene Med*. 2007;9(8):649–658.
35. Yang P, Singh J, Wettig S, Foldvari M, Verrall RE, Badea I. Enhanced gene expression in epithelial cells transfected with amino acid-substituted gemini nanoparticles. *Eur J Pharm Biopharm*. 2010;75(3):311–320.
36. Mohammed-Saeid W, Michel D, El-Aneed A, Verrall RE, Low NH, Badea I. Development of lyophilized gemini surfactant-based gene delivery systems: influence of lyophilization on the structure, activity and stability of the lipoplexes. *J Pharm Pharm Sci*. 2012;15(4):548–567.
37. Zhang Y, Hong H, Cai W. PET tracers based on Zirconium-89. *Curr Radiopharm*. 2011;4(2):131–139.
38. Deri MA, Zeglis BM, Francesconi LC, Lewis JS. PET imaging with ^{89}Zr: from radiochemistry to the clinic. *Nucl Med Biol*. 2013;40(1):3–14.
39. Vugts DJ, van Dongen GA. (89)Zr-labeled compounds for PET imaging guided personalized therapy. *Drug Discov Today Technol*. 2011;8(2–4):e53–e61.
40. Turner DC, Gruner SM. X-ray diffraction reconstruction of the inverted hexagonal (HII) phase in lipid-water systems. *Biochemistry*. 1992;31(5):1340–1355.
41. Vosjan MJ, Perk LR, Visser GW, et al. Conjugation and radiolabeling of monoclonal antibodies with zirconium-89 for PET imaging using the bifunctional chelate p-isothiocyanatobenzyl-desferrioxamine. *Nat Protoc*. 2010;5(4):739–743.
42. Perk LR, Vosjan MJ, Visser GW, et al. p-Isothiocyanatobenzyl-desferrioxamine: a new bifunctional chelate for facile radiolabeling of monoclonal antibodies with zirconium-89 for immuno-PET imaging. *Eur J Nucl Med Mol Imaging*. 2010;37(2):250–259.
43. Almofti MR, Harashima H, Shinohara Y, Almofti A, Baba Y, Kiwada H. Cationic liposome-mediated gene delivery: biophysical study and mechanism of internalization. *Arch Biochem Biophys*. 2003;410(2):246–253.
44. Wasungu L, Hoekstra D. Cationic lipids, lipoplexes and intracellular delivery of genes. *J Control Release*. 2006;116(2):255–264.
45. Mehnert W, Mäder K. Solid lipid nanoparticles: production, characterization and applications. *Adv Drug Deliv Rev*. 2001;47(2–3):165–196.
46. Tseng YC, Xu Z, Guley K, Yuan H, Huang L. Lipid-calcium phosphate nanoparticles for delivery to the lymphatic system and SPECT/CT imaging of lymph node metastases. *Biomaterials*. 2014;35(16):4688–4698.
47. Al-Dulaymi MA, Chitanda JM, Mohammed-Saeid W, et al. Di-peptide-modified gemini surfactants as gene delivery vectors: exploring the role of the alkyl tail in their physicochemical behavior and biological activity. *AAPS J*. 2016;18(5):1168–1181.
48. Zeglis BM, Davis CB, Aggeler R, et al. Enzyme-mediated methodology for the site-specific radiolabeling of antibodies based on catalyst-free click chemistry. *Bioconjug Chem*. 2013;24(6):1057–1067.
49. Keliher EJ, Yoo J, Nahrendorf M, et al. 89Zr-labeled dextran nanoparticles allow in vivo macrophage imaging. *Bioconjug Chem*. 2011;22(12):2383–2389.
50. Wang H-E, Yu H-M, Lu Y-C, et al. Internal radiotherapy and dosimetric study for 111In/177Lu-pegylated liposomes conjugates in tumor-bearing mice. *Nucl Instrum Meth A*. 2006;569(2):533–537.
51. Bae YH, Park K. Targeted drug delivery to tumors: myths, reality and possibility. *J Control Release*. 2011;153(3):198–205.
52. Kang CM, Koo HJ, Lee S, Lee KC, Oh YK, Choe YS. 64Cu-Labeled tetraiodothyroacetic acid-conjugated liposomes for PET imaging of tumor angiogenesis. *Nucl Med Biol*. 2013;40(8):1018–1024.
53. van der Geest T, Laverman P, Gerrits D, et al. Comparison of three remote radiolabelling methods for long-circulating liposomes. *J Control Release*. 2015;220(Pt A):239–244.
54. Sakurai F, Terada T, Yasuda K, Yamashita F, Takakura Y, Hashida M. The role of tissue macrophages in the induction of proinflammatory cytokine production following intravenous injection of lipoplexes. *Gene Ther*. 2002;9(16):1120–1126.
55. Longmire M, Choyke PL, Kobayashi H. Clearance properties of nano-sized particles and molecules as imaging agents: considerations and caveats. *Nanomedicine (Lond)*. 2008;3(5):703–717.
56. Kagan L, Gershkovich P, Wasan KM, Mager DE. Dual physiologically based pharmacokinetic model of liposomal and nonliposomal amphotericin B disposition. *Pharm Res*. 2014;31(1):35–45.
57. Polyak A, Palade EA, Balogh L, et al. In vitro and biodistribution examinations of Tc-99m-labelled doxorubicin-loaded nanoparticles. *Nucl Med Rev Cent East Eur*. 2011;14(2):55–62.
58. Pérez-Campaña C, Gómez-Vallejo V, Puigivila M, et al. Biodistribution of different sized nanoparticles assessed by positron emission tomography: a general strategy for direct activation of metal oxide particles. *ACS Nano*. 2013;7(4):3498–3505.
59. Wilhelm S, Tavares AJ, Dai Q, et al. Analysis of nanoparticle delivery to tumours. *Nat Rev Mater*. 2016;1(5):16014.
60. Lee H, Hoang B, Fonge H, Reilly RM, Allen C. In vivo distribution of polymeric nanoparticles at the whole-body, tumor, and cellular levels. *Pharm Res*. 2010;27(11):2343–2355.
61. Liu TW, Macdonald TD, Jin CS, et al. Inherently multimodal nanoparticle-driven tracking and real-time delineation of orthotopic prostate tumors and micrometastases. *ACS Nano*. 2013;7(5):4221–4232.
62. Mohammed-Saeid W, Chitanda J, Al-Dulaymi M, Verrall R, Badea I. Design and Evaluation of RGD-Modified Gemini Surfactant-Based Lipoplexes for Targeted Gene Therapy in Melanoma Model. *Pharm Res*. 2017;34(9):1886–1896.

Supplementary materials

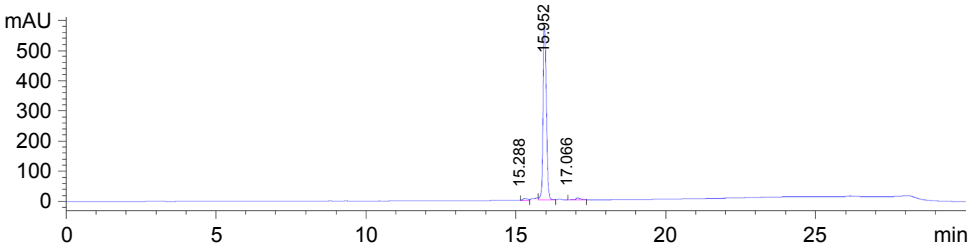

Figure S1 HPLC chromatogram of the deferoxamine-modified gemini surfactant detected with absorbance detector at 254 nm. (Using Agilent 1200 series HPLC system).

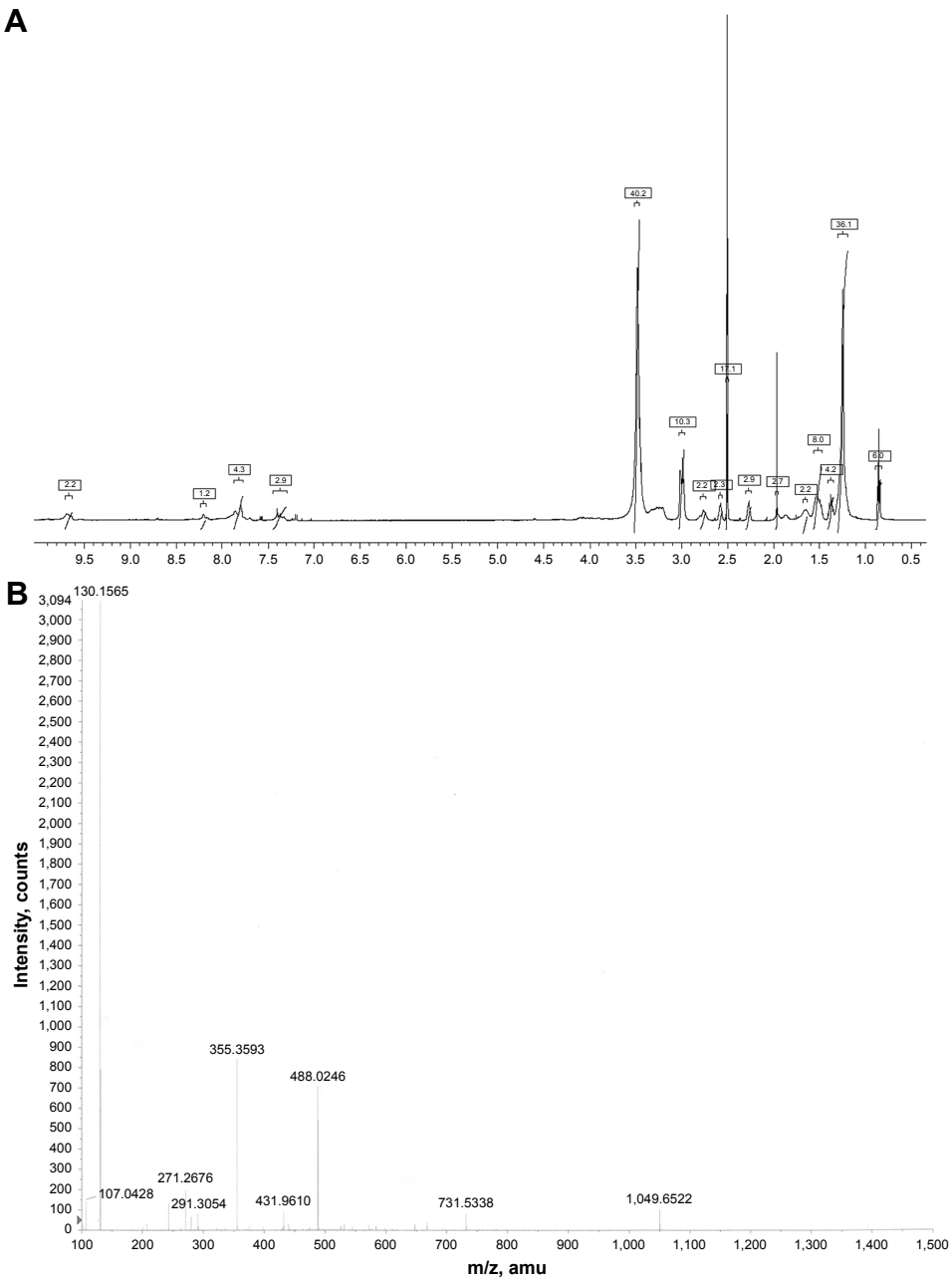

Figure S2 (**A**) NMR 12-7NGK-Deferoxamine-12 of (**B**) mass spectrum of 12-7NGK-Deferoxamine-12. Found mass: 731.5338 $[M]^{2+}/2$ m/z: calculated mass: 731.5232.

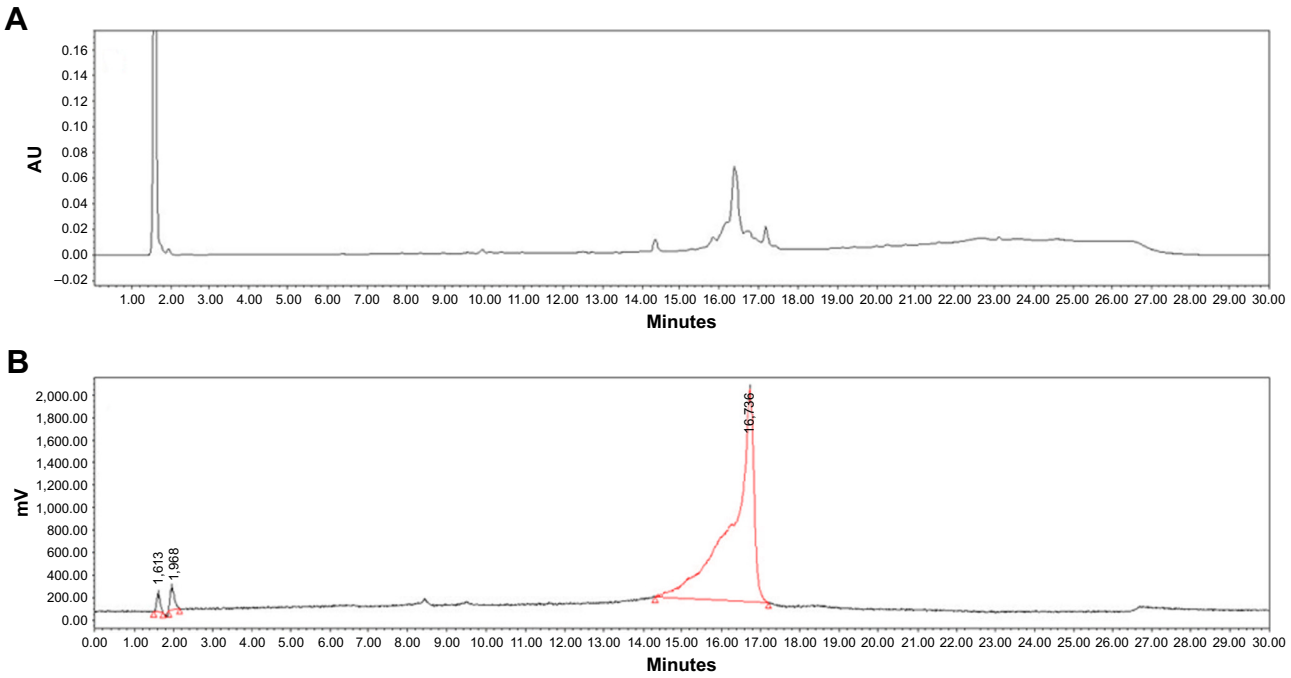

Figure S3 HPLC chromatogram of ^{89}Zr labeled gemini surfactant detected with absorbance detector at 254 nm (**A**) and Radio-HPLC Detector (**B**). (Using Waters 2796 HPLC System). N.B. free ^{89}Zr was eluted with the solvent.